Key Engineering Materials
ISSN: 1662-9795, Vol. 786, pp 400-408
doi:10.4028/www.scientific.net/KEM.786.400

Submitted: 2018-04-25
Revised: 2018-06-02
Accepted: 2018-06-03
Online: 2018-10-31

Two-Step Synthesis of Copper Sulfide-Graphene Counter Electrode for CdS Quantum Dot Sensitized Solar Cells

Amr Hessein[1a*] and Ahmed Abd El-Moneim[2]

[1]Department of Mathematical and Physical Engineering, Faculty of Engineering (Shoubra), Benha University, Cairo 11614, Egypt

[2]Department of Materials Science and Engineering, Egypt-Japan University of Science and Technology, New Borg El Arab City, Alexandria 21934, Egypt

[*]amr.ahmed@ejust.edu.eg; amrhessein7@yahoo.com

Keywords: Copper sulfide; graphene; QDSSC; counter electrode; polysulfide electrolyte.

Abstract. The development of high performance and cost-effective counter electrode (CE) is a persistent objective in order to convey the quantum dot sensitized solar cell (QDSSC) from laboratories to markets benches. In the current study, we present a simple two-step approach for fabricating a highly efficient CE for QDSSC composes from copper sulfide (CuS) nanoparticles and reduced graphene oxide (RGO) mixture. The two-step approach gave us the opportunity to synthesis pure cupric sulfide (CuS) nanoparticles; in the first step and with smaller particle size before mixing with graphene. In the second step, different ratios from CuS and RGO were prepared and tested as counter electrodes in QDSSCs. The preliminary results obtained from CdS-QDSSCs employing CuS-RGO CE demonstrate that high dependency on the content of the CuS nanoparticles into the counter electrode. As high as 2.62% power conversion efficiency was exhibited by replacing 75% graphene content by CuS nanoparticles into the counter electrode. The obtained results were explained by means of electrochemical measurements of the fabricated CEs along with morphological and structural properties of the prepared nanocomposites.

1. Introduction

Semiconductor nanoparticles (Quantum dots QDs) had showed outstanding optical and optoelectronic properties compared to its counterpart bulk materials [1]. Properties such as larger light harvesting, bandgap tunability, multiple carrier generation were experimentally proved for QDs [2]. The Quantum dot sensitized solar cell (QDSSC) that belonging to the third generation of photovoltaic is low-cost with simple fabrication is able to efficiently benefit from the merits of QDs to overcome the operational and fabrication limitations from the previous two generations [3]. However, the power conversion efficiency of QDSSC is still lower than photovoltaics from the first and second generations. The lack of appropriate counter electrode is considered as one of the important reason causing the inferior performance of QDSSC and also limits its large scale commercial applications [4]. High electrochemical activity, long-term chemical stability and durability besides low-cost and ease of fabrication are the prerequisites for high performance counter electrode [5].

To date research has been devoted to find out efficient and low cost alternative CEs for QDSSCs from earth abundant elements to replace the expensive noble metal Pt CE. Various materials including carbon-based materials [6–9], metal chalcogenides [4,10–14], and conducting polymers [15,16], were explored as CEs in QDSSCs. Among the tested materials, the CEs fabricated from copper sulfides (Cu_xS) showed a promising photovoltaic performance with accepted electrocatalytic activity towards the reduction of (S^{2-}/S_x^{2-}) electrolyte compared to the other materials [4]. However, its charge carrier mobility and stability was not satisfactory, and the PCE of the cells based on sole Cu_xS CE is degraded to about 60–70% of its initial value after the first two hours of the cell assembly [17]. Therefore, it is needed to develop an innovative method for fabricating electro active and stable Cu_xS film on FTO substrate, meeting the requirements of large

scale production. Graphene the newest member in the family of carbon materials had been showed exceptional electrical, optical, and chemical properties that could be employed to fulfill the perquisites of efficient CE needed for QDSSCs [18].

In this regard, this work is dedicated to build up a high performance graphene-based CE for QDSSC from graphene and the electrocatalytic active copper sulfides (Cu_xS) nanoparticles (NPs). Graphene was used as a conductive matrix to support Cu_xS NPs for providing a faster electrons transfer rate and larger number of active sites for the electrolyte reduction. The two-step method is based on obtaining the nanocomposites from mixing the separately prepared graphene and Cu_xS NPs. This approach gave us the opportunity to synthesis pure cupric sulfide (CuS) NPs, the most electrocatalytic active phase between Cu_xS phases, and with smaller particle size.

2. Experimental

2.1 Counter electrode preparation

RGO was prepared through the chemical reduction of aqueous graphene oxide solution using hydrazine hydrate [19]. The copper sulfide (CuS) nanoparticles were prepared according to our previous report from the reaction of aqueous solutions of copper (II) nitrate [$Cu(NO_3)_2{\cdot}3H_2O$] and sodium sulfide ($Na_2S{\cdot}9H_2O$) aqueous solutions in the presence of ethylene glycol (EG) [20]. In order to fabricate homogeneous CuS- RGO nanocomposite, a proper amount of the RGO was mixed with different ratios (25, 50, 75%) of the as-prepared CuS NPs and grounded for 15 min in agate mortar. After that, 45 mg form CuS- RGO nanocomposite and 5 mg of PVDF (10% wt: wt) were uniformly dispersed in 1 ml of NMP by mild sonication for two hours. CuS-RGO thin film CEs were formed directly on FTO substrate by drop casting 10 µl from the CuS-RGO dispersion on pre-cleaned FTO substrate of an exposed area of 1 cm^2 defined by adhesive tape. All the fabricated CEs were dried at 110 ^oC for at least 12 hours in an electric drying oven under normal atmospheric conditions. For the purpose of comparison, RGO, pure CuS NPs and Cu_2S/brass CEs were also fabricated.

2.2 QDSSCs device fabrication

The QDSSC devices were fabricated by assembling CdS QDs-sensitized photoanodes and CEs into sandwich-type solar cells using Parafilm as a spacer between the two electrodes. The photoanodes comprise 10.5±0.2 µm mesoporous TiO_2 layer with a dense TiO_2 blocking layer underneath; were sensitized with CdSe QDs for 10 SILAR cycles and passivated with ZnS QDs [21]. A regenerative polysulfide electrolyte (S^{2-}/S_x^{2-}) composed of 1 M Na_2S, 1 M S, and 0.1 M KCl in distilled water was used to fill the space between the two electrodes. The active areas of all tested devices were defined at fixed value of 0.28 cm^2 by clamping a shadow mask to the solar cell surface using binder clips.

2.3 Measurements and characterization

The morphology of samples were characterized by field emission scanning electron microscopy (FESEM) using (SEM, JEOL JEM-6500F). X-ray powder diffraction (XRD) was measured using Rigaku diffractometer (RINT 2100 PC). Raman scattering spectra were measured using a laser wavelength of 532 nm on Raman microscope (RAMANtouch). The photovoltaic measurements were performed using a solar simulator (San-Ei Electric XES-40S1) at AM 1.5 at 1 sun illumination intensity (100 mW/cm^2), and the current density–voltage (*J-V*) data were recorded using a source meter unit (Keithley SMU 2400). The electrochemical measurements were carried out on an electrochemical workstation (CH Instruments 660E).

3. Results and Discussions

3.1 Morphologies and structures of counter electrodes

The phase purity and crystallinity of the as prepared CuS NPs were investigated by the X-ray powder diffraction XRD, and the collected diffraction pattern is shown in Fig. 1(a). All the obtained diffraction peaks in the pattern are well matched with the hexagonal covellite phase of cupric

sulfide (JCPDS Card No. 00-006-0464). The XRD measurement also did not detect any diffraction peaks related to any non-stoichiometric copper sulfide Cu_xS phases, which indicate the feasibility of our method for synthesising pure covellite CuS NPs. The average particle size was estimated to be about ~24 nm using Debby Scherrer's equation based on the FWHM of the most intense reflection peak (110) with Bragg's diffraction angle of 47.9° [20]. This estimated particle size of CuS NPs is in well matching with from the FESEM surface morphology result presented in Fig 1(b), which shows the formation of aggregated CuS NPs with irregular shapes between 20 and 30 nm in size.

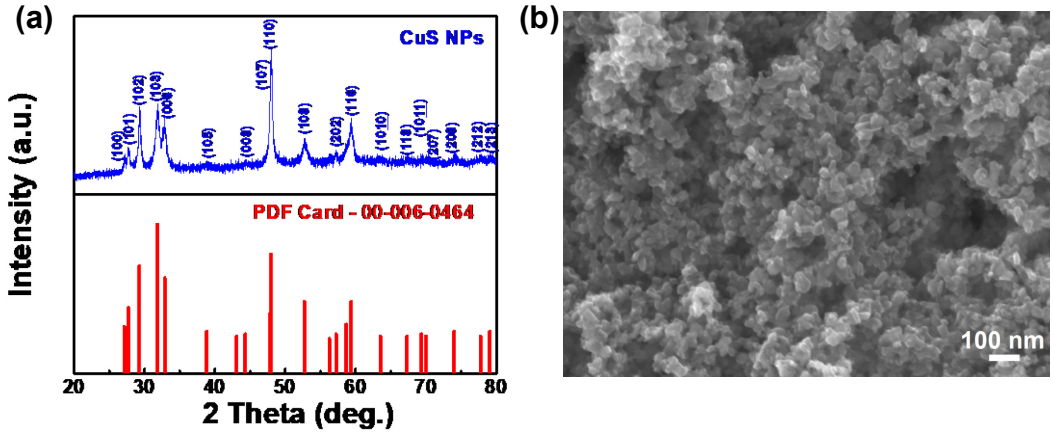

Fig. 1. (a) XRD, and (b) FESEM micrograph of the prepared CuS NPs.

Fig. 2 show the FESEM micrographs of the fabricated CuS- RGO CEs taken at kX 30 magnification. The slight coverage with uniform loading of the few-layers RGO flakes with CuS NPs can be clearly shown from Fig. 2(a) for the CE mixed with 25% CuS NPs. The coverage was increased when the doping ratio has increased to 50%, and a complete coverage of the RGO flakes with CuS NPs was achieved with the 75% mixing level as revealed in Fig. 2(c). This obtained full coverage of RGO surface with catalytic active CuS NPs is supposed to boost the electrochemical activity of the fabricated CEs [5].

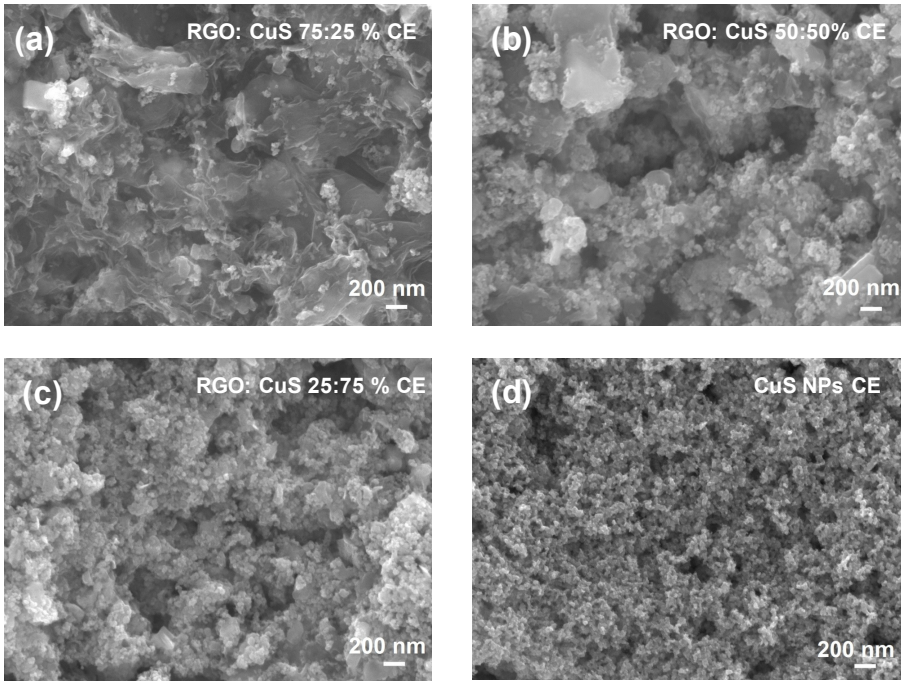

Fig. 2. FESEM micrographs of the CuS-RGO CEs with different loading amounts of CuS NPs.

The incorporation between RGO and CuS NPs in the nanocomposite was also examined by Raman scattering spectroscopy as shown in Fig. 3. The Raman spectrum of the prepared CuS NPs

showed the two well known distinct peaks at 471 cm^{-1} and 261 cm^{-1} attributed to the S-S stretching and Cu-S vibration modes in covellite CuS phase, respectively [22]. A noticeable increase in the intensity of the 471 cm^{-1} Raman peak for CuS NPs with respect to D and G peaks of RGO can be seen by increasing the amount of CuS NPs dopant. This result is a good confirmation on the homogeneous merging between RGO and CuS NPs in the nanocomposite which in consistency with the results from the FESEM micrographs.

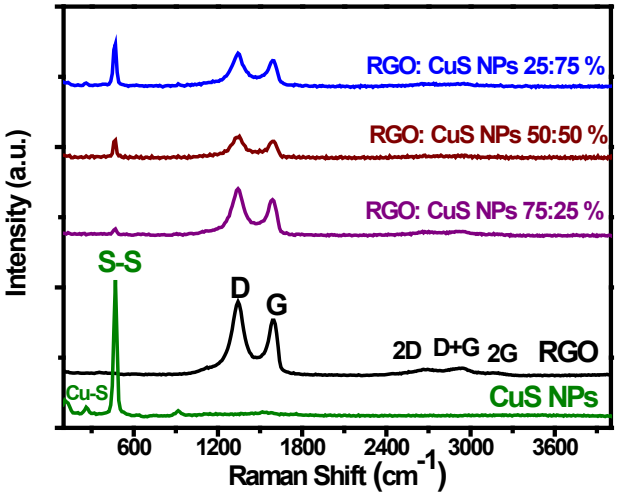

Fig. 3. The Raman scattering spectra of the different CuS-RGO CEs**.**

3.2 Electrochemical measurements for counter electrodes

In QDSSCs, the electrons are collected from the external circuit via the CE. The collected electrons used to regenerate the oxidized polysulfide ions in the electrolyte. The electrons collection efficiency and injection kinematics into the electrolyte are crucial factors in determination the overall performance on QDSSC devices. Therefore, electrochemical measurements such as cyclic voltammetry (CV), electrochemical impedance spectroscopy (EIS) commonly employed to carefully investigate the electrochemical activity of QDSSCs electrodes [23]. Fig. 4(a) shows the cyclic voltammograms of all the fabricated CEs symmetrical cells measured at a scan rate of 50 mV/s. The negative current density in CV curve is the cathodic current generated by the reduction process of polysulfide (S_x^{2-}) ions to sulfide (S^{2-}) ions at the CE surface, while the positive anodic current represent the oxidation process [24]. Hence, the value of the cathodic current density (J_{red}) is directly related to the electrochemical activity of the tested CE for S_x^{2-} ions reduction. Clearly seeing from the CV voltammograms a sharp increase in the J_{red} of RGO CE from 13 mA/cm^2 to 46.76 mA/cm^2 achieved by adding 25% CuS NPs. The further increase in the amount of CuS NPs was resulted in an increase in the J_{red} values. The maximum J_{red} value of 64.87 mA/cm^2 was yielded from the RGO:CuS 25:75 % CE, which is higher than 57.79 mA/cm^2 obtained from bare CuS NPs CE and much higher than 37.87 mA/cm^2 from the Cu_2S/brass CE. These results indicates a superior catalytic activity of our developed RGO:CuS 25:75 % CE for S_x^{2-} ions reduction due to the effective integration between RGO and CuS NPs in the CE.

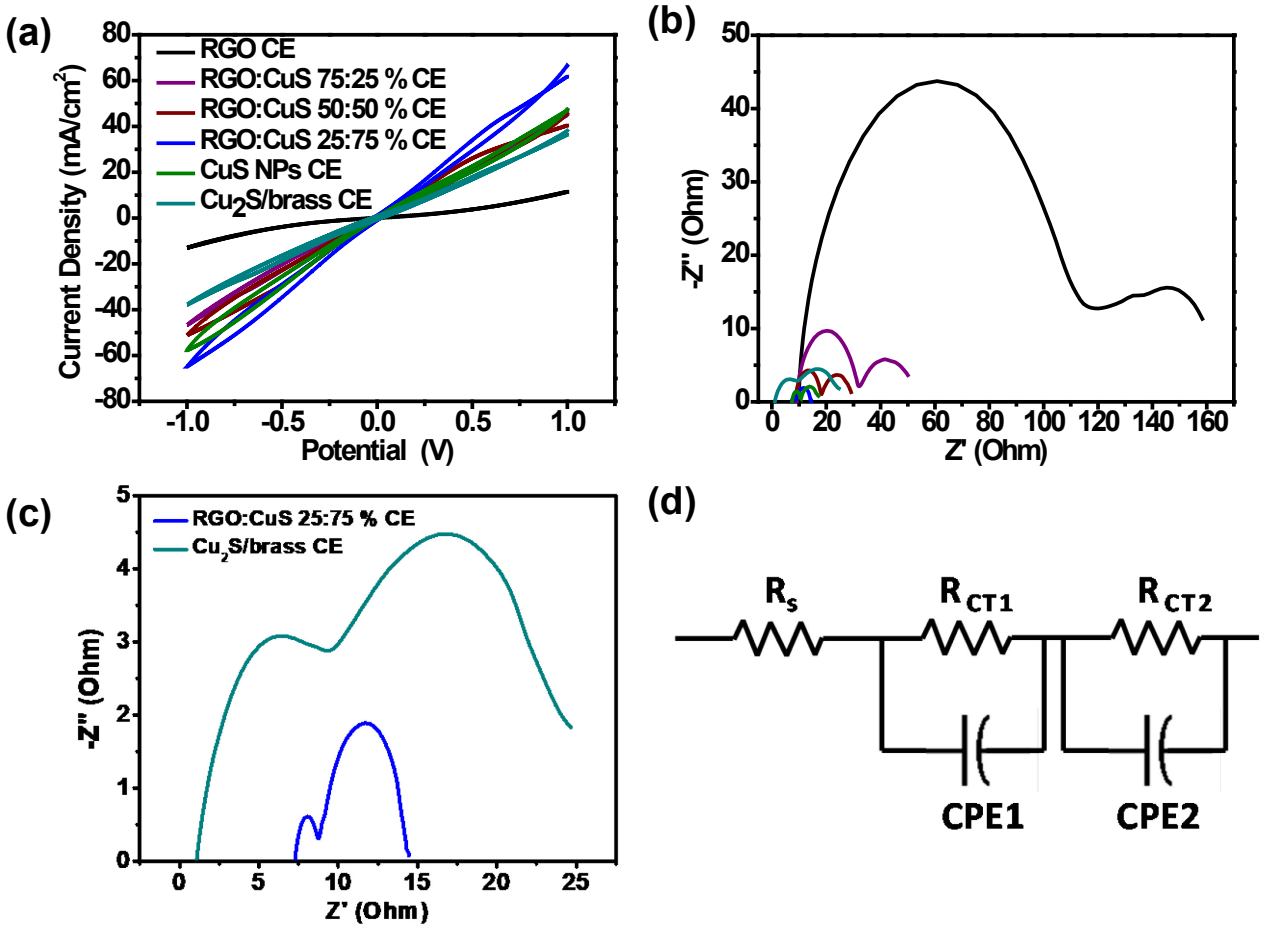

Fig. 4. (a) CV, (b) EIS, (c) low range EIS and (d) equivalent circuit of all fabricated CEs.

The EIS for the different CEs symmetric cells were recorded in frequency range from 0.1 Hz to 100 kHz at 0 V bias voltage and 20 mV AC amplitude and the obtained Nyquist plots are shown in Fig. 4(b) & (c). The EIS data were fitted to the equivalent circuit shown in Fig. 4(d) using Zsimpwin software and the fitted impedance parameters are summarized in Table 1. In this equivalent circuit, the series resistance (R_s) is given by the nonzero intercept at the real axis and comprises the bulk resistance of the CE material and the sheet resistance of the supporting substrate. R_{CT1} and the constant phase element (CPE1) are the charge transfer resistance and charging double layer capacitance at the solid-solid interface, whereas R_{CT2} and CPE2 are the charge transfer resistance and charging capacitance at the electrolyte-CE interface, respectively circuit [10].

Seeing from the fitted EIS parameters, replacing 25% of RGO with CuS NPs into the CE resulted in acute decrease in the R_{CT1} (97.18 Ω) and R_{CT2} (62.27 Ω) for the RGO CE to lower values of 23.13 Ω and 17.87 Ω, respectively

Table 1. The calculated electrochemical parameters for all fabricated CEs.

Counter Electrode	J_{red} (mA/cm^2)	R_s (Ω)	R_{CT1} (Ω)	R_{CT2} (Ω)
RGO CE	13.01	9.58	97.18	62.27
RGO:CuS 75:25 % CE	46.76	9.1	23.13	17.86
RGO:CuS 50:50 % CE	51.1	8.43	9.87	10.83
RGO:CuS 25:75 % CE	64.87	7.36	1.48	5.71
CuS NPs CE	57.59	7.52	2.9	6.95
Cu_2S/brass CE	37.87	1.12	7.04	17.29

The lowest R_{CT1} (1.48 Ω) and R_{CT2} (5.71 Ω) was obtained from the RGO:CuS 25:75 % CE, much lower than the commonly used Cu_2S/brass CE that showed higher R_{CT1} (7.04 Ω) and R_{CT2} (17.29 Ω). The lower values R_{CT1} and R_{CT2} reflect the favourable charge transfer across FTO/RGO:CuS and RGO:CuS/electrolyte interfaces with in the RGO:CuS 25:75 % CE, and its higher electrocatalytic activity as well. Also, the reduction in R_s values of RGO:CuS CEs indicate the better binding between the CE active material and the FTO substrate.

In Brief, efficient CEs for (S^{2-}/S_x^{2-}) electrolyte reduction was obtained by the successful incorporation between the conductive RGO sheets (25%) and the catalytic active CuS NPs (75%). The fabricated RGO:CuS 25:75 CE showed a superior electrocatalytic activity, exceeding that from the bare CuS NPs CE and the commonly used Cu_2S/brass CE.

3.3 Photovoltaic Performance of QDSSC devices

The *J-V* characteristic curves of CdS QDSSC devices assembled with CuS-RGO CEs with different ratios of CuS NPs are shown in Fig. 5(a), and the obtained photovoltaic parameters are presented in Table 4-6. The doping of the RGO CE with only 25% CuS NPs resulted in large increase in V_{OC} of 0.419 V and J_{SC} of 5.97 mA/cm^2 to much higher values of 0.4702 V and 8.388 mA/cm^2, respectively. This increase associated with an increase in the FF to 40.6% led to nearly 100% increase in the PCE based on RGO CE to reach 1.6%. The further increase in the CuS NPs ratio to 50% improved the FF to 45.9% and the PCE to 2.26%. The best photovoltaic performance was exhibited by the CE that prepared with 75% CuS NPs. Although the RGO:CuS 25:75 % CE showed lower V_{OC} (0.545 V) than the device assembled with pure CuS NPs (0.589 V), however the significantly higher J_{SC} (10.62 mA/cm^2) was the essential reason for the remarkable high PCE of 2.62% achieved. On the other side, J_{SC} of 8.72 mA/cm^2 and PCE of 2.3% were obtained from QDSSC based on the pure CuS NPs CE.

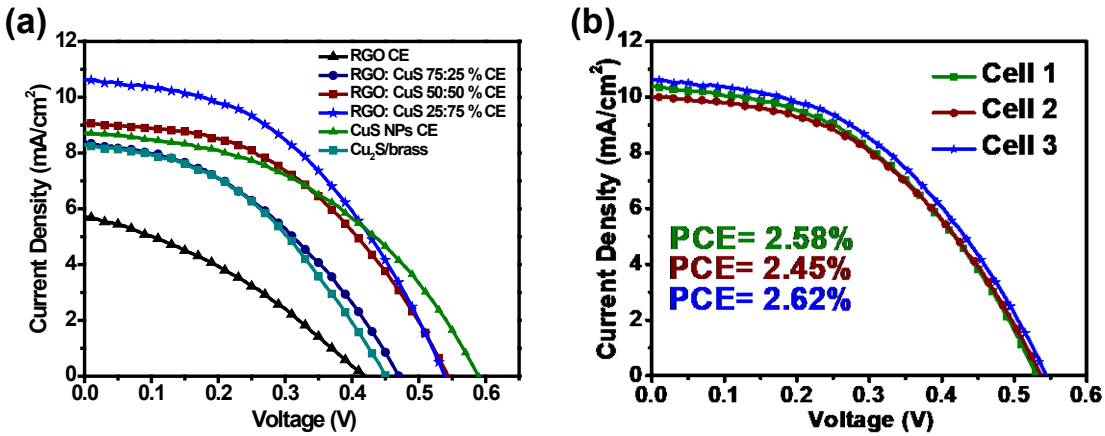

Fig. 5. (a) The *J-V* curves of CdS QDSSCs based on the different CEs, (b) the reproducibility test data.

These attained photovoltaic results are consistent with the electroactivity trend of all fabricated CEs evaluated from the electrochemical measurements, which expected the effective integration between RGO and CuS NPs in CuS-RGO 25:75 % CE makes the S_x^{2-} ions reduction more preferable. Worthy to mention, the highly obtained 2.62% PCE from the best CuS-RGO CE are 67% higher than the PCE form the application of the Cu_2S/brass as CE. The reproducibility of the high performance of RGO:CuS 25:75 % CE was also confirmed from three CdS QDSSC assembled devices as revealed in Fig. 5(b). This result indicates the ability of our developed two-step approach in producing a superior performance and reproducible CuS- RGO CE for QDSSC applications.

Table 2. The photovoltaic parameters of CdS QDSSC devices based on the different CEs.

Counter electrode	V_{OC} (V)	J_{SC} (mA/cm^2)	FF (%)	PCE (%)
RGO CE	0.419	5.97	34.5	0.85
RGO:CuS 75:25 % CE	0.470	8.388	40.6	1.60
RGO:CuS 50:50 % CE	0.544	9.07	45.9	2.26
RGO:CuS 25:75 % CE	0.545	10.62	45.2	2.62
CuS NPs CE	0.589	8.72	44.9	2.30
Cu_2S/brass CE	0.451	8.28	42.2	1.57

Furthermore, the photostability of the fabricated devices was tested by monitoring the J_{SC} coming out from QDSSC devices under continuous one sun illumination for 3h and the change in J_{SC} is shown in Fig. 6. The highly obtained J_{SC} for CdS QDSSC device based on the RGO:CuS 25:75 % CE maintains it value during the 180 min testing course. This result is mainly attributed to the use of CuS active NPs; the most stable form of copper sulphides, in addition to wrapping the NPs with the chemically stable graphene sheets. On the contrary, the QDSSC devices based on the Cu_2S/brass CE suffered from instability problems. A very sharp decrease in J_{SC} was observed during the first hour of the test, and complete failure of the cell occurred after 2 h of testing due to the dissociation of Cu_2S thin film from the substrate and poisoning the photoanode.

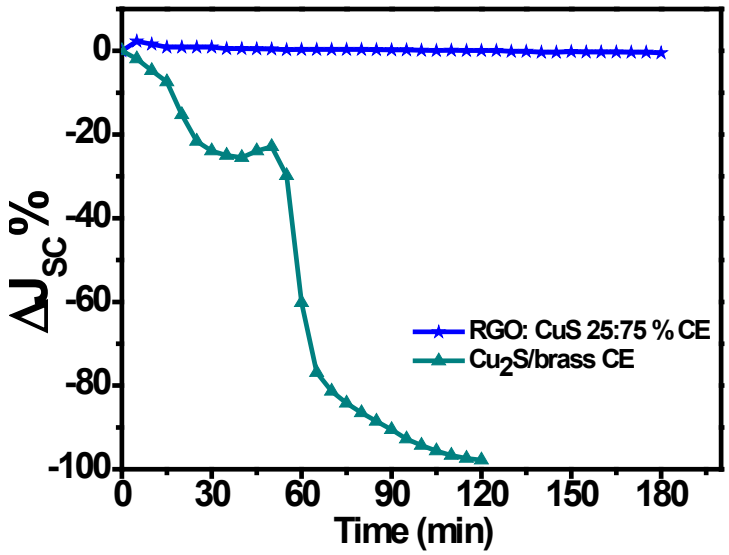

Fig. 6. The percentage change in the JSC of CdS QDSSCs based on RGO:CuS 25:75 %, and Cu_2S/brass CEs under light soaking for 180 min.

4. Conclusions

In summary, we have prepared an efficient and highly stable CE for QDSSC applications from CuS NPs and RGO via the effective two-step approach. Pure covellite CuS NPs were first prepared with facile low-temperature method. After that, the electrocatalyst nanocomposites were prepared by mixing different weight ratios of CuS NPs and RGO with the aid of PVDF as a polymeric binder. The CEs were fabricated by the simple and productive drop-casting technique directly on the FTO substrates. The CdS QDSSCs based on the optimized two-step CuS-RGO CE showed a higher PCE of 2.62% and an impressive photocurrent of 10.62 mA/cm^2 with perfect reproducibility too. This obtained outstanding result overcome the result from similar QDSSC device fabricated using the state-of-the-art Cu_xS/brass CE that is only attained 1.57% PCE. Finally, the excellent photovoltaic performance, the low production cost, and ease of fabrication, imply that our two-step approach for fabricating graphene based CE is convenient for QDSSC applications.

5. Acknowledgments

The authors are grateful to professor Kazunari Matsuda, Institute of Advanced Energy (IAE), Kyoto University and professor A. Wakamiya, Institute for Chemical Research (ICR), Kyoto University, for their kind help and support for performing and finishing this work.

References

[1] A.J. Nozik, Quantum dot solar cells, 14 (2002) 115–120.

[2] S. Rühle, M. Shalom, A. Zaban, Quantum-dot-sensitized solar cells., Chemphyschem. 11 (2010) 2290–2304. doi:10.1002/cphc.201000069.

[3] P. V. Kamat, Quantum dot solar cells. The next big thing in photovoltaics, J. Phys. Chem. Lett. 4 (2013) 908–918. doi:10.1021/jz400052e.

[4] I. Hwang, K. Yong, Counter Electrodes for Quantum-Dot-Sensitized Solar Cells, ChemElectroChem. 2 (2015) 634–653. doi:10.1002/celc.201402405.

[5] K. Meng, G. Chen, K.R. Thampi, Metal chalcogenides as counter electrode materials in quantum dot sensitized solar cells: a perspective, J. Mater. Chem. A. 3 (2015) 23074–23089. doi:10.1039/C5TA05071E.

[6] V.-D. Dao, Y. Choi, K. Yong, L.L. Larina, H.-S. Choi, Graphene-based nanohybrid materials as the counter electrode for highly efficient quantum-dot-sensitized solar cells, Carbon N. Y. 84 (2015) 383–389. doi:10.1016/j.carbon.2014.12.014.

[7] Q. Zhang, Y. Zhang, S. Huang, X. Huang, Y. Luo, Q. Meng, D. Li, Application of carbon counter electrode on CdS quantum dot-sensitized solar cells (QDSSCs), Electrochem. Commun. 12 (2010) 327–330. doi:10.1016/j.elecom.2009.12.032.

[8] G.S. Paul, J.H. Kim, M.S. Kim, K. Do, J. Ko, J.S. Yu, Different hierarchical nanostructured carbons as counter electrodes for Cds quantum dot solar cells, ACS Appl. Mater. Interfaces. 4 (2012) 375–381. doi:10.1021/am201452s.

[9] J. Selvaraj, S. Gupta, S. Delacruz, V. Subramanian, Role of reduced graphene oxide in the critical components of a CdS-sensitized TiO_2-based photoelectrochemical cell, ChemPhysChem. 15 (2014) 2010–2018. doi:10.1002/cphc.201402275.

[10] H. Zhang, H. Bao, X. Zhong, Highly efficient, stable and reproducible CdSe-sensitized solar cells using copper sulfide as counter electrodes, J. Mater. Chem. A. 3 (2015) 6557–6564. doi:10.1039/C5TA00068H.

[11] Y. Chen, X. Zhang, Q. Tao, W. Fu, H. Yang, S. Su, Y. Mu, L. Zhou, M. Li, High catalytic activity of a PbS counter electrode prepared via chemical bath deposition for quantum dots-sensitized solar cells, RSC Adv. 5 (2015) 1835–1840. doi:10.1039/C4RA08076A.

[12] H. Geng, L. Zhu, W. Li, H. Liu, L. Quan, F. Xi, X. Su, FeS/nickel foam as stable and efficient counter electrode material for quantum dot sensitized solar cells, J. Power Sources. 281 (2015) 204–210. doi:10.1016/j.jpowsour.2015.01.182.

[13] H.J. Kim, T. Bin Yeo, S.K. Kim, S.S. Rao, A.D. Savariraj, K. Prabakar, C.V.V.M. Gopi, Optimal-temperature-based highly efficient NiS counter electrode for quantum-dot-sensitized solar cells, Eur. J. Inorg. Chem. 2014 (2014) 4281–4286. doi:10.1002/ejic.201402026.

[14] H. Salaramoli, E. Maleki, Z. Shariatinia, M. Ranjbar, CdS/CdSe quantum dots co-sensitized solar cells with Cu_2S counter electrode prepared by SILAR, spray pyrolysis and Zn–Cu alloy methods, J. Photochem. Photobiol. A Chem. 271 (2013) 56–64. doi:10.1016/j.jphotochem.2013.08.006.

[15] M.H. Yeh, C.P. Lee, C.Y. Chou, L.Y. Lin, H.Y. Wei, C.W. Chu, R. Vittal, K.C. Ho, Conducting polymer-based counter electrode for a quantum-dot-sensitized solar cell (QDSSC) with a polysulfide electrolyte, Electrochim. Acta. 57 (2011) 277–284. doi:10.1016/j.electacta.2011.03.097.

[16] S. Abdulalmohsin, J. Armstrong, J.B. Cui, CdS nanocrystal-sensitized solar cells with polyaniline as counter electrode, J. Renew. Sustain. Energy. 4 (2012) 43108. doi:10.1063/1.4737133.

[17] J.H. Zeng, D. Chen, Y.F. Wang, B. Bin Jin, Graphite Powder Film-Supported Cu_2S Counter Electrodes for Quantum Dot Sensitized Solar Cells, J. Mater. Chem. C. 3 (2015) 12140–12148. doi:10.1039/C5TC02101D.

[18] A.B. Suriani, M.D. Nurhafizah, A. Mohamed, M.H. Mamat, M.F. Malek, M.K. Ahmad, A. Pandikumar, N.M. Huang, Enhanced photovoltaic performance using reduced graphene oxide assisted by triple-tail surfactant as an efficient and low-cost counter electrode for dye-sensitized solar cells, Optik (Stuttg). 139 (2017) 291–298. doi:10.1016/j.ijleo.2017.04.025.

[19] A. Hessein, A.A. El-moneim, Developing Cost Effective Graphene Conductive Coating and its Application as Counter Electrode for CdS Quantum Dot Sensitized Solar Cell, Proc. World Congr. New Technol. (NewTech 2015). (2015) 307–1.

[20] A. Hessein, F. Wang, H. Masai, K. Matsuda, A.A. El-Moneim, Improving the stability of CdS quantum dot sensitized solar cell using highly efficient and porous CuS counter electrode, J. Renew. Sustain. Energy. 9 (2017) 23504. doi:10.1063/1.4978346.

[21] A. Hessein, F. Wang, H. Masai, K. Matsuda, A.A. El-moneim, One-step fabrication of copper sulfide nanoparticles decorated on graphene sheets as highly stable and efficient counter electrode for CdS-sensitized solar cells, 55 (2016) 1–8. doi:10.7567/JJAP.55.112301.

[22] C.S. Kim, S.H. Choi, J.H. Bang, New insight into copper sulfide electrocatalysts for quantum dot-sensitized solar cells: Composition-dependent electrocatalytic activity and stability, ACS Appl. Mater. Interfaces. 6 (2014) 22078–22087. doi:10.1021/am505473d.

[23] I.R.C. Rose, A.J. Rajendran, Exploring the effect of morphology of Ni and Co doped cadmium selenide nanoparticles as counter electrodes in dye-sensitized solar cell, Optik (Stuttg). 155 (2018) 63–73. doi:10.1016/j.ijleo.2017.10.148.

[24] M. Ye, X. Wen, N. Zhang, W. Guo, X. Liu, C. Lin, In situ growth of CuS and $Cu_{1.8}S$ nanosheet arrays as efficient counter electrodes for quantum dot-sensitized solar cells, J. Mater. Chem. A. 3 (2015) 9595–9600. doi:10.1039/C5TA00390C.